Lattice constants and cohesive energies of alkali, alkaline-earth, and transition metals: Random phase approximation and density functional theory results

Laurids Schimka,[*] René Gaudoin, Jiří Klimeš, Martijn Marsman, and Georg Kresse

Faculty of Physics, Universität Wien, and Center for Computational Materials Science, Sensengasse 8/12, A-1090 Wien, Austria

We present lattice constants and cohesive energies of alkali, alkaline earth, and transition metals using the correlation energy evaluated within the adiabatic-connection fluctuation-dissipation (ACFD) framework in the random phase approximation (RPA) and compare our findings to results obtained with the meta-GGA functional revTPSS and the gradient corrected PBE (Perdew-Burke-Ernzerhof) functional and the PBEsol functional (PBE reparametrized for solids), as well as a van der Waals (vdW) corrected functional optB88-vdW. Generally, the RPA reduces the mean absolute error in the lattice constants by about a factor 2 compared to the other functionals. Atomization energies are also on par with the PBE functional, and about a factor 2 better than with the other functionals. The study confirms that the RPA describes all bonding situations equally well including van der Waals, covalent, and metallic bonding.

PACS number(s): 31.15.A−

I. INTRODUCTION

Benchmarking theoretical methods against experimental data is common practice widely adopted within the density functional theory[1,2] (DFT) community, in particular, when introducing new functionals. However, remarkably few systematic results are available for the transition-metal series. Although these elements are partly covered in Refs. 3 and 4, a concise study covering all elements using modern density functionals is so far not available. The tests presented here close this gap and include transition metals of the $3d$, $4d$, and $5d$ series, as well as alkali and alkaline earth and coinage metals. We show results for lattice constants and cohesive energies obtained with several different approximations to the exchange correlation energy: the widely applied generalized gradient approximation (GGA) of Perdew, Burke, and Ernzerhof[5] (PBE) and its reparametrized version for solids PBEsol,[6] the recently published meta-GGA revTPSS (Tao-Perdew-Staroverov-Scuseria),[7,8] the optB88-vdW (Ref. 9) functional which uses the nonlocal correlation functional of Dion *et al.*[10] with the exchange functional fitted to reproduce weak interactions in the gas phase, and finally the random phase approximation in the adiabatic-connection fluctuation-dissipation (ACFD) framework.[11–13] The local density approximation has not been included in this study since it underestimates the lattice constants of $3d$ metals significantly, strongly overestimates the atomization energies, and does not yield accurate results for magnetic transition metals.

Furthermore, all experimental values are corrected for the effect of zero-point vibrational energies, which were calculated at the DFT level applying a force constant approach.[14] Where necessary, the lattice constants were also extrapolated from available finite-temperature data to 0 K. Independent of the actual results for the here investigated functionals, these data will serve as a useful reference for future work.

One reason why the $3d$, $4d$, and $5d$ series have been rarely considered as a benchmark might be that most of the semilocal functionals are not particularly good in describing the different bonding situations encountered in these series. Although the alkali and alkaline earth metals are usually considered to be prototypical metals that can be well described even using second-order perturbation theory and a free-electron-gas reference,[15] a sizable bonding contribution also stems from van der Waals bonding, in particular, for the soft alkali metals. This contribution originates from the semicore p and to a lesser extent semicore s states, and can modify the lattice constants by up to 2%–3%.[16] As the d filling increases along the series, the bonding changes from s- and p-like bonding in alkali and alkaline earth metals to bonding dominated by the d electrons. It is commonly assumed that d bonding includes a sizable fraction of covalent bonding with bonding linear combinations of d states below the Fermi level and antibonding linear combinations above the Fermi level.[17]

Other challenging materials are the metallic $3d$ elements which exhibit a fairly small band width and are expected to show strong fluctuations in the ground state. Specifically, ferromagnetic Fe, Co, and Ni are known to be difficult for density functionals, as exemplified by the many attempts to include correlations beyond the mean field.[18–21] In summary, transition metals include contributions from different kinds of bonding: van der Waals-type bonding between closed semicore s and p shells, van der Waals bonding from closed semicore d states towards the end of the series (Cu, Ag, and in particular Au), free-electron-like metallic bonding for alkali, alkaline earth metals and the coinage metals, as well as covalent d bonding.

As we will also see in this work, the general shortcoming of semilocal functionals in describing bonding between closed shells results in large errors towards the beginning and the end of the series: the "classical" PBE functional is indeed unsatisfactory. With the advent of new functionals that include the kinetic energy density, the situation has slightly improved, as we will confirm here for the meta-GGA functional revTPSS. However, our main focus is on the random phase approximation, which should capture all important bonding contributions accurately.[22–24] As a side line, we will also show results for ferromagnetic Fe, Co, and Ni and thereby assess the accuracy of the random phase approximation for magnetic elements.

TABLE I. PAW potentials used in this work. The second column indicates the states treated as valence states. The local potential was generated by replacing the all-electron potential by a soft potential within the cutoff radius r_{loc} (a.u.), which is provided in the "r_{loc}" column. The number of partial waves and projectors for different angular momentum numbers l is specified in columns 4–7. The energy cutoff E_{cut} specifies the VASP "default" cutoff in eV for DFT calculations usually guaranteeing convergence of absolute energies to few meV per electron. This cutoff is determined by the largest wave vector of the spherical Bessel functions that are used when the all electron partial wave is replaced by a soft pseudopartial wave.

	Valence	r_{loc}	s	p	d	f	E_{cut} (eV)
K	$3s\,3p\,4s$	1.2	3	2	1		249
Ca	$3s\,3p\,4s$	1.2	3	2	1		281
Sc	$3s\,3p\,4s\,3d$	1.2	3	2	1	1	285
Ti	$3s\,3p\,4s\,3d$	1.2	3	2	1	1	286
V	$3s\,3p\,4s\,3d$	1.1	3	2	1	1	323
Fe	$3s\,3p\,4s\,3d$	1.0	4	3	1	1	364
Co	$3s\,3p\,4s\,3d$	1.1	4	3	1	1	364
Ni	$3s\,3p\,4s\,3d$	1.1	4	3	1	1	413
Cu	$3d\,4s$	1.5	2	2	2	1	417
Rb	$4s\,4p\,5s$	1.8	3	2	2	1	221
Sr	$4s\,4p\,5s$	1.8	3	2	2	1	225
Y	$4s\,4p\,5s\,4d$	1.8	3	2	2	1	229
Zr	$4s\,4p\,5s\,4d$	1.6	3	2	2	1	282
Nb	$4s\,4p\,5s\,4d$	1.6	3	2	2	1	286
Mo	$4s\,4p\,5s\,4d$	1.6	3	2	2	1	312
Tc	$4s\,4p\,5s\,4d$	1.6	3	2	2	1	318
Ru	$4s\,4p\,5s\,4d$	1.6	3	2	2	1	321
Rh	$4s\,4p\,5s\,4d$	1.6	3	2	2	1	320
Pd	$4d\,5s$	1.6	2	2	2	2	251
Ag	$4d\,5s$	1.4	2	2	2	2	250
Cs	$5s\,5p\,6s$	1.8	2	2	2	2	198
Ba	$5s\,5p\,6s$	1.8	2	2	2	2	237
Hf	$5s\,5p\,6s\,5d$	1.6	3	2	2	1	283
Ta	$5s\,5p\,6s\,5d$	1.6	3	2	2	1	286
W	$5s\,5p\,6s\,5d$	1.6	3	2	2	1	317
Re	$5s\,5p\,6s\,5d$	1.6	3	2	2	1	317
Os	$5s\,5p\,6s\,5d$	1.6	3	2	2	1	320
Ir	$5s\,5p\,6s\,5d$	1.6	3	2	2	1	320
Pt	$5s\,5p\,6s\,5d$	1.6	3	2	2	1	324
Au	$5d\,6s$	1.6	2	2	2	1	300

II. TECHNICAL DETAILS

All calculations were performed using the Vienna *ab initio* simulation package (VASP),[26,27] applying the projector-augmented wave (PAW) potentials[28,29] listed in Table I. The potentials correspond to the GW potentials distributed with the VASP package. These potentials are slightly more accurate than the standard VASP potentials, although the DFT lattice constants agree within 0.15% with the lattice constants obtained using other PAW potentials with a similar set of valence orbitals.[30] Furthermore, we note that freezing the semicore states by placing them into the core increases the DFT lattice constants by up to 0.5% for the early transition metals (Sc, Ti, V, Y, Nb, Mo).

Details for the construction of the pseudopartial waves are discussed in Ref. 31. This specific construction results in fairly soft potentials requiring only modest plane wave cutoffs, as listed in Table I. Since the density functional theory calculations are comparatively cheap, the energy cutoff has been set to 800 eV for the revTPSS and optB88-vdW calculations and to 1000 eV for the PBE and PBEsol calculations. For PBE and PBEsol, results at 1000 and 800 eV are identical, guaranteeing that all reported results are fully converged with respect to the plane wave basis set for semilocal functionals. At 800 eV, the more costly revTPSS and optB88-vdW calculations are also essentially exact, as confirmed by repeating some calculations at a higher plane wave cutoff. For the significantly more expensive RPA calculations, we have set the energy cutoff to 1.5 times the "default" energy cutoff listed in Table I. All RPA calculations were performed using the PBE orbitals and PBE one-electron energies (RPA@PBE), and no attempts to obtain self-consistent results were made.

The Brillouin zone (BZ) was sampled by $15 \times 15 \times 15$ k points for the bulk calculations with the density functionals. For the RPA, the BZ sampling was increased from $6 \times 6 \times 6$ over $8 \times 8 \times 8$ to $10 \times 10 \times 10$ k points where k-point convergence was observed, except for Fe, where the k-point set had to be increased to $16 \times 16 \times 16$ k points. For the hcp structures we used the ideal c/a ratio and a $10 \times 10 \times 10$ k-point grid. Overall, we found that this setup ensures an accuracy of about 0.25% in the lattice constants (better than 1% in the volume). The equilibrium volumes were determined using a seven-point fit to a Birch-Murnaghan equation of state, where the volume in the calculations was varied by $\pm15\%$. The bulk modulus is not reported here. Because of noise in the RPA data, the changes in the bulk moduli from one to the next k-point set sometimes exceed 10% (Cu, Ag, Au), although changes of 5% are more common. Furthermore, the bulk moduli show nothing unexpected and follow the usual trend: if the volume is overestimated, the bulk modulus tends to be underestimated and *vice versa*.

For the calculations of the atoms, a $14 \times 15 \times 16$ Å^3 cell was used for the density functional theory calculations. The ground states of the atoms were calculated by seeking the lowest-energy configuration allowing for spin polarization and breaking of the spherical symmetry, but disregarding spin-orbit coupling. All symmetry-broken ground-state configurations were characterized by orbital occupancies of 1 (occupied) or 0 (unoccupied) only. In some cases, we started the DFT calculations from different starting points, to guarantee that the lowest-energy configuration was correctly determined. In most (but not all) cases, the DFT ground-state configuration agrees with the experimental observations (see Sec. III B). For the RPA, three calculations at three different volumes were performed ($7 \times 8 \times 9$ Å^3, $8 \times 9 \times 10$ Å^3, and $9 \times 10 \times 11$ Å^3) and the values were extrapolated to the isolated atom limit. The exact exchange energy (evaluated also using PBE orbitals) was evaluated for supercells of $10 \times 11 \times 12$ Å^3, $11 \times 12 \times 13$ Å^3, and $12 \times 13 \times 14$ Å^3 and also extrapolated to the isolated atom limit (for alkali and alkali earth metals even larger unit cells were used). Depending on the convergence corrections, the exact exchange energy can show spurious finite-size errors of the order 1/volume before this residual correction, whereas the correlation energy shows residual finite-size errors of the order 1/volume squared before correction.[22] Except for Ti, the present RPA calculations for atoms are usually based

on the PBE ground-state orbitals, disregarding that the true RPA atomic ground state could correspond to a different atomic configuration. For titanium, the RPA calculations were initiated from a DFT-PBE calculation with the atomic configuration $3d^2 4s^2$ (total spin moment $2\mu_B$) compatible to experiment. This lowered the atomic RPA energy significantly.

The zero-point vibration corrections to the lattice constants and atomization energies were calculated from density functional theory using the same procedure as outlined in Ref. 32. The vibrational frequencies were calculated using a $2 \times 2 \times 2$ supercell of the conventional (cubic) unit cell. The BZ sampling was done with $8 \times 8 \times 8$ k points. A similar energy cutoff as in the RPA calculations was chosen, yielding essentially converged results in the phonon frequencies (errors are below 1% upon further increase of the energy cutoff). For elements with a hexagonal close-packed structure (hcp), the vibrational contributions were estimated using a more convenient face centered cubic (fcc) structure. In tests, we found that applying the fcc instead of the hcp structure yields identical results up to the third digit in the energy (eV).

III. RESULTS AND DISCUSSION

A. Equilibrium volumes

Figure 1 shows the relative error of the equilibrium volumes with respect to the experimental values extrapolated where necessary to 0 K. All metals were considered in their nonmagnetic states, except for Fe, Co, and Ni, which were considered in the ferromagnetic bcc (Fe) and ferromagnetic fcc (Co and Ni) structures. We have subtracted the effect of the zero-point vibrational energies from the experimental data. In the tables and figures, the elements are ordered by ascending atomic number. Cr and Mn have been excluded from this study. Mn exhibits a complicated antiferrimagnetic structure and would require significant efforts in the RPA.[36] Cr is antiferromagnetic, with a very strong change of the local magnetic moment around the equilibrium volume (at least in density functional theory). In the RPA, this would require us to scan the energy landscape as a function of the volume
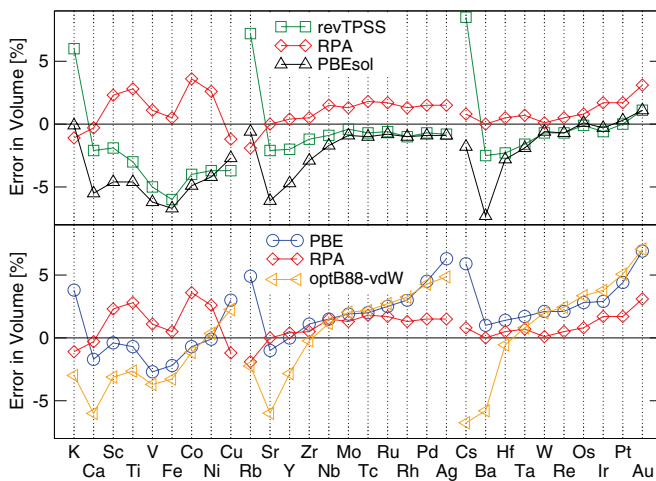
FIG. 1. (Color online) Relative error in volume compared to experimental data from which the effects of the zero-point energy as well as the thermal effects (where necessary) were subtracted.

and magnetic moment, an effort beyond the scope of this study. For the other ferromagnetic metals (bcc Fe, fcc Co, and fcc Ni), we have simply used the PBE density functional theory orbitals and one-electron eigenvalues to determine the exact exchange energy, as well as the correlation energy in the random phase approximation. For the magnetic materials, the magnetic moment is therefore fixed to the values determined in the ground-state DFT-PBE calculations.

We will start our discussion with the well-established PBE functional. The PBE functional (blue circles) works fairly well across the series, with the errors being noticeably larger for the alkali metals and the coinage metals (Cu, Ag, and Au). The errors in the volumes are particularly sizable for Rb (4.9%), Ag (6.3%), Cs (5.9%), and Au (6.9%). It is also well established that PBE yields fairly accurate $3d$ lattice constants, but the lattice constants for the $4d$ and $5d$ elements are systematically overestimated. What is particularly unsatisfactory is the increase of the lattice constants along the series with increasing d-band filling. We found a similar increase also for other pure density functionals, for instance, PBEsol (see Fig. 1) or AM05. Furthermore, a similar behavior is quite generally found as the atomic number increases.[3] The origin for this is not fully understood. Most likely, the conventional density functionals fail to describe important electronic correlations between neighboring sites. Along this line of arguments, the large error for K, Rb, and Cs, as well as the coinage metals Cu, Ag, and Au, is then related to the neglect of correlation effects between closed semicore s and p states for alkali metals, and between the almost filled d shells for Cu, Pd, Ag, Pt, and Au.

The RPA (red diamonds) yields much improved results. Most notable is the decrease of the lattice constants for the alkali metals as well as coinage metals. We relate this to the fact that the random phase approximation can account for the correlation between closed shells (van der Waals bonding),[22] allowing for an accurate description of the correlation between the semicore s and p states for K, Rb, and Cs and the filled d shells for Cu, Ag, and Au. A slight tendency towards too large lattice constants with increasing d-band filling prevails in the RPA, but this might be also related to some systematic deficiency of the PAW data sets for correlated calculations. Specifically, we note that the RPA results are sensitive to the description of the unoccupied states, and although we include partial waves for f states for most elements, we have not made attempts to include g partial waves as well. Visual inspection of the scattering properties, however, indicates that the g scattering properties are very accurately described by the local potential. The more likely explanation for the increase in the lattice constant is some residual self-interaction error within the d shell, which will necessarily increase with d-band filling.

The results for the $3d$ metals are also satisfactory for the RPA. For Co and Ni, we find a tendency towards too large volumes, but with volume errors of 3%–4% the errors remain acceptably small. For Fe, the RPA energy-volume curve is very peculiar, with a double-well structure shown in Fig. 2. We note that this behavior becomes more apparent when $20 \times 20 \times 20$ k points are used, and the corresponding calculations were performed using otherwise less stringent convergence criteria than for the other calculations. The first minimum is deeper, and corresponds very well with the experimentally observed
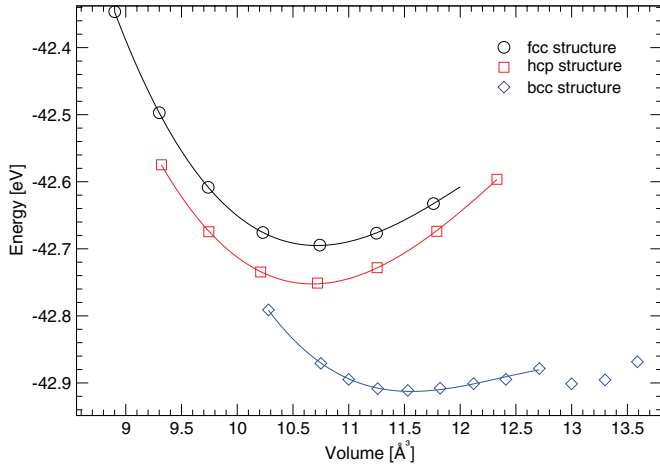
FIG. 2. (Color online) Energy-volume curve for nonmagnetic fcc, nonmagnetic hcp, and ferromagnetic bcc iron as obtained for RPA.

lattice constant, whereas the second minimum occurs at larger volumes. At this volume, the DFT ground-state calculations that we use to determine the orbitals and occupancies show a spin of $2.5\mu_B$, close to a Hund's rule ferromagnet which we believe to be related to the existence of the second minimum. In passing, we note that no such minimum was observed for the other ferromagnetic transition metals Co and Ni. We also determined the energy difference between magnetic bcc Fe and nonmagnetic hcp and fcc Fe using the RPA and found values of $\Delta E_{\text{bcc-hcp}} = -130$ meV and $\Delta E_{\text{bcc-fcc}} = -180$ meV. This confirms that the magnetic phase is more stable than competing nonmagnetic phases. Furthermore, the energy differences are slightly larger than for the PBE functional ($\Delta E_{\text{bcc-hcp}} = -83$ meV, $\Delta E_{\text{bcc-fcc}} = -153$ meV). We predict a transition pressure of 32 GPa for a pressure-induced transition from ferromagnetic bcc to nonmagnetic hcp, but note that the lowest-energy hcp structure might possess an antiferromagnetic or antiferrimagnetic spin order possibly lowering its energy.[33] Hence, we do not consider the overestimation of the transition pressure compared to experiment to be an issue.

In summary, the RPA yields excellent results with a quite clear tendency towards, on average, 1%–2% too large volumes, as we already observed in our previous studies for *s*- and *p*-bonded systems. Compared to PBE, the improvements are also clearly visible in the statistical mean relative error (MRE) and mean absolute relative error (MARE) summarized in Table II. The MRE and MARE drop by almost a factor 2 from PBE to RPA, and the small MARE is particularly noteworthy.

The revTPSS results are shown as green squares in the first panel of Fig. 1. We will first concentrate on the 4*d* and 5*d* metals. Disregarding Rb and Cs, it is astounding how closely the revTPSS curve follows the RPA. Furthermore, revTPSS yields about 2% smaller volumes than RPA improving the agreement with experiment and, most notably, revTPSS exhibits also no significant slope with increasing *d*-band filling. Considering the design principles of revTPSS, we can understand this behavior. The revTPSS functional uses the kinetic energy density to distinguish spatial regions where the electron density stems from a single orbital only from those where the density is made up by the sum of the density of many (one-electron)

orbitals. When the density is made up by many orbitals, the functional behaves very similar to the PBEsol functional, whereas in spatial regions where the density originates from one orbital only, a functional form is used that largely removes self-interaction errors. This allows the revTPSS functional to recover the exchange and correlation energy of the hydrogen atom almost exactly. As the *d* band becomes filled, revTPSS hence gradually switches from a "one-electron" description to a "many-electron" description, becoming gradually identical to the PBEsol functional at roughly half filling (compare Fig. 1). Below half filling, the self-interaction free form increases the lattice constants compared to PBEsol, counteracting the slope in the PBE and PBEsol functionals. This explains the very respectable performance of revTPSS for 4*d* and 5*d* metals. For the alkali metals, however, large errors prevail, and these are certainly related to the neglect of correlation effects from the filled semicore states that semilocal functionals can not handle by construction.[16]

The 3*d* metals are another issue. Errors for Fe are unfortunately fairly large, and the volume almost drops to PBEsol values (see also Ref. 8). In this case, the functional is too "PBEsol" like, as the *d* shell is almost entirely filled. What was beneficial for the filled 4*d* and 5*d* shells has clearly a negative impact on the magnetic 3*d* metals. This also significantly increases the MARE over that for the RPA, resulting in, overall, an only modest improvement over PBE.

Finally, we turn to the optB88-vdW functional[9] which uses the vdW-DF correlation functional of Dion *et al.*[10] and a modified B88 exchange functional.[37] The results for some of the materials have been published before,[38] namely, the alkali and alkaline earth metals as well as the late *d* metals (Cu, Rh, Pd, and Ag). It was observed that this functional gives similar results as PBE for the late *d* metals, while too small equilibrium volumes were obtained for the alkali and alkaline earth metals. This follows the trend already observed here for the other GGA-based functionals (PBE and PBEsol). However, the slope in the difference to experiment from left to right is even larger than for PBE and PBEsol. We checked that the reason for the increase in the slope is the vdW correlation functional: replacing the vdW correlation by the PBE correlation recovers the behavior for other semilocal functionals. We conclude that the vdW functional most likely overestimates dispersion contributions with particularly sizable errors for the soft alkali metals (and to a lesser extent alkaline earth metals).

B. Atomization energies

The accurate prediction of atomization energies is a difficult challenge to density functional theory methods, as well as many-electron methods. For transition metals, the situation is particularly severe since transition metals are "strongly" correlated with many almost isoenergetic low-energy configurations in the Hartree-Fock approximation. Since the true many-electron wave function for the ground state is then a mixture of many Slater determinants, often multiconfiguration methods are needed to make accurate predictions for transition-metal atoms and their compounds. Despite the multiconfigurational many-electron wave function, density functionals very often yield reasonably accurate answers for the atomization energy of transition-metal solids.[4]

TABLE II. Theoretical equilibrium volumes for PBE, revTPSS, and RPA. The columns marked with % report the relative error with respect to experimental data corrected for zero-point vibrational effects. These are shown in the last column, while the uncorrected results are given in parentheses. If not otherwise stated, corrected experimental values are from this work. All elements were considered in the nonmagnetic state, except for Fe, Co, and Ni (ferromagnetic).

		PBE	%	PBEsol	%	revTPSS	%	optB88-vdW	%	RPA	%	Experiment
K	bcc	73.51	3.8	70.70	−0.1	75.05	6.0	68.67	−3.0	70.02	−1.1	70.79[a] (71.32)[a]
Ca	fcc	42.15	−1.7	40.53	−5.5	41.97	−2.1	40.31	−6.0	42.74	−0.3	42.88[a] (43.09)[a]
Sc	hcp	24.63	−0.4	23.58	−4.6	24.24	−1.9	23.95	−3.1	25.28	2.3	24.72 (25.00)[b]
Ti	hcp	17.39	−0.7	16.71	−4.6	16.99	−3.0	17.06	−2.6	18.00	2.8	17.52 (17.66)[b]
V	bcc	13.45	−3.2	12.93	−6.2	13.05	−5.0	13.28	−3.7	13.96	1.1	13.78 (13.88)[b]
Fe	bcc	11.36	−2.2	10.83	−6.7	10.92	−6.0	11.23	−3.3	11.67	0.5	11.61[a] (11.71)[a]
Co	fcc	10.86	−0.7	10.40	−4.9	10.50	−4.0	10.81	−1.1	11.33	3.6	10.94 (11.08)[b]
Ni	fcc	10.78	−0.1	10.34	−4.2	10.39	−3.7	10.83	0.4	11.07	2.6	10.79 (10.94)[b]
Cu	fcc	11.97	3.0	11.31	−2.7	11.19	−3.7	11.88	2.3	11.48	−1.2	11.62[c] (11.69)[c]
Rb	bcc	90.99	4.9	86.22	−0.6	93.00	7.2	84.79	−2.2	85.11	−1.9	86.73[a] (87.10)[a]
Sr	fcc	54.53	−1.0	51.71	−6.1	53.95	−2.1	51.79	−6.0	55.11	0.0	55.09[a] (55.31)[a]
Y	hcp	32.84	0.0	31.29	−4.7	32.19	−2.0	31.90	−2.8	32.95	0.4	32.83 (33.18)[b]
Zr	hcp	23.37	1.1	22.45	−2.9	22.85	−1.2	23.07	−0.2	23.25	0.5	23.12 (23.27)[b]
Nb	bcc	18.14	1.5	17.56	−1.7	17.71	−0.9	18.08	1.2	18.14	1.5	17.87[a] (17.90)[a]
Mo	bcc	15.79	1.9	15.35	−0.9	15.44	−0.4	15.81	2.0	15.70	1.3	15.49[a] (15.54)[a]
Tc	hcp	14.45	2.0	14.02	−1.0	14.06	−0.7	14.48	2.2	14.43	1.8	14.17 (14.30)[d]
Ru	hcp	13.77	2.5	13.33	−0.8	13.36	−0.6	13.81	2.7	13.67	1.7	13.44 (13.55)[b]
Rh	fcc	14.06	3.0	13.51	−1.0	13.52	−1.0	14.09	3.2	13.83	1.3	13.65[c] (13.70)[c]
Pd	fcc	15.21	4.5	14.43	−0.9	14.46	−0.7	15.18	4.3	14.77	1.5	14.56[c] (14.61)[c]
Ag	fcc	17.81	6.3	16.61	−0.9	16.62	−0.8	17.57	4.8	17.01	1.5	16.76[c] (16.84)[c]
Cs	bcc	116.65	5.9	108.16	−1.8	119.51	8.5	102.69	−6.8	110.96	0.8	110.12[e] (110.45)[e]
Ba	bcc	63.17	1.0	58.01	−7.3	60.99	−2.5	58.95	−5.8	62.59	0.0	62.58[a] (62.76)[a]
Hf	hcp	22.43	1.4	21.50	−2.8	21.62	−2.3	22.00	−0.6	22.22	0.5	22.12 (22.25)[d]
Ta	bcc	18.25	1.7	17.61	−1.9	17.66	−1.6	18.09	0.8	18.09	0.7	17.95[a] (17.98)[a]
W	bcc	16.11	2.1	15.68	−0.6	15.67	−0.7	16.10	2.0	15.79	0.1	15.78[a] (15.81)[a]
Re	hcp	14.92	2.1	14.52	−0.7	14.51	−0.7	14.97	2.4	14.69	0.5	14.61 (14.71)[b]
Os	hcp	14.29	2.8	13.91	0.1	13.88	−0.1	14.37	3.4	14.01	0.8	13.90 (13.99)[b]
Ir	fcc	14.47	2.9	14.02	−0.3	13.98	−0.6	14.59	3.8	14.30	1.7	14.06[a] (14.15)[a]
Pt	fcc	15.63	4.4	15.02	0.3	14.99	0.0	15.74	5.1	15.24	1.7	14.98[a] (15.01)[a]
Au	fcc	17.92	6.9	16.95	1.1	16.95	1.1	17.94	7.1	17.28	3.1	16.76[a] (16.79)[a]
MRE			1.9		−2.5		−0.8		0.0		1.0	
MARE			2.5		2.6		2.4		3.2		1.3	

[a]Reference 3.
[b]Reference 35.
[c]Reference 32.
[d]Reference 34.
[e]Reference 4.

Here, we define the atomization energy (or cohesive energy) of a material M with N atoms in a unit cell as

$$E_{\text{Atm}}(\text{M}) = \frac{1}{N} \left\{ \sum_{\text{atoms}} E(\text{X}) - E(\text{M}) \right\}. \qquad (1)$$

$E(\text{M})$ is the total energy of the solid and $E(\text{X})$ denotes the corresponding energy of the constituent atoms. With this definition, positive errors correspond to an overbinding, whereas negative errors correspond to underbinding. It is clear from Fig. 3 that PBE performs quite reasonably for the atomization energies. It is also quite remarkable that, with few exceptions, the atomic electronic configurations predicted by PBE agree with experiments (compare Table III). These exceptions are Ti, V, and W. For Ti, the exact

exchange energy (EXX) and the RPA atomic energy are considerably lower when the experimental configuration is chosen as starting point for the RPA calculations, which can be achieved by fixing the magnetic moment in the preceding DFT calculations to $2\mu_B$ (triplet). Therefore, RPA and EXX predict an atomic electronic configuration in agreement with experiment, whereas PBE fails to predict the correct atomic ground state of Ti. For V, PBE, and RPA, as well as EXX, all predict the wrong atomic electronic configuration, and for W we where unable to stabilize the experimental $5d^4 6s^2$ configuration, as our electronic-structure code always ended up in the $5d^5 6s^1$ configuration.

For PBE, errors are always close to zero and hardly ever exceed 0.5 eV. The RPA inherits this good overall performance
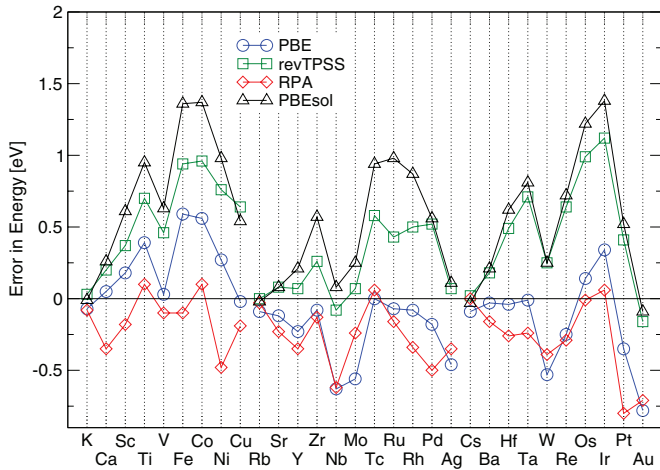
FIG. 3. (Color online) Error of the theoretic atomization energy in eV compared to experiment. Positive value means that the atomization energy is overestimated by a given functional.

from PBE, in particular for the mean absolute error (MAE). The statistical errors compiled in Table III indicate that RPA shows the usual underestimation of the binding energies also observed for other elements in the periodic table.[24] It has been demonstrated that this error is significantly reduced by adding the second-order screened exchange (SOSEX) contribution,[25] but the corresponding calculations are presently not possible for metallic systems. Furthermore, outliners with particularly large errors are Ni, Nb, and Pt. These three atoms are characterized by PBE one-electron band gaps that are smaller than 0.15 eV in the atomic ground state. This small band gap causes a single strong transition in the excitation spectrum, shifting the RPA atomic energies to too negative values. The magnitude of this small one-electron band gap depends on the DFT functional, and increases by a factor 1.5 for the revTPSS functional. When the revTPSS functional is used to generate the orbitals and one-electron energies for the RPA calculations, the atomization energies of Ni, Nb, and Pt agree slightly better with experiment (Ni 4.25, Nb 7.15, Pt 5.14), whereas the atomization energies of other elements hardly change by more than 50 meV. The improvement is, however, modest, and the small changes suggest that the atomization energies are not very sensitive to the choice of the initial DFT functional.

Remarkably, the RPA as well as all density functionals exhibit minima in the binding curve for close to half filling (Nb and W) and for an entirely filled d band (Ni, Pd, Ag, Pt, and Au). Note that the d band contains more electrons for equivalent 4d elements than 5d elements (e.g., Mo versus W) since the 6s shell is pulled down by relativistic effects increasing its occupancy in the 5d series. Hence, the minimum for half filling occurs slightly earlier in the 4d elements (Nb) than in the 5d elements (W).

One possible reason for this systematic variation in the atomization energies and the agreement between RPA and PBE is that the interpolation of the correlation energy between the nonmagnetic and fully spin-polarized case (known from quantum Monte Carlo simulations) is based on the RPA correlation energy for a partially spin-polarized electron gas.[39] Possibly, this underestimates the correlation energy of atoms

with partially spin-polarized shells, with accurate results only obtained at full spin polarization and zero spin polarization. Finally, we observe that the 3d metals behave differently than the 4d and 5d metals. Specifically, the PBE overbinds all 3d metals compared to experiment (recall the too small PBE lattice constants), whereas the RPA yields excellent agreement with experiment, with a slight tendency towards too small binding energies as for the 4d and 5d series.

The performance of revTPSS and PBEsol for the atomization energies is somewhat disappointing. The mean error increases from -0.07 eV for PBE to 0.41 for revTPSS. We note that a similar behavior has already been observed for other solids in our recent work.[8] As opposed to semiconductors and insulators where the revTPSS atomization energies are very good, the revTPSS atomization energies of metals are generally close to PBEsol values and significantly too large. We can understand this along the same line of arguments already discussed above: in metals, and specifically in transition metals with a largely filled d shell, the total charge density is the sum of several one-electron orbitals. In this case, the revTPSS functional behaves very similar to the PBEsol functional. Although this was clearly beneficial for the lattice constants, it undesirably increases the atomization energies to that of the PBEsol functional. We finally note that PBEsol and revTPSS seem to be accurate for some elements, for instance, the alkali metals, Au, and Ag, as well as Pd and Pt, elements that are often included in benchmark data sets. This highlights that too limited test sets might be misleading in judging the overall quality of a functional.

IV. SUMMARY AND CONCLUSIONS

The here considered test set of 30 alkali, alkaline earth, transition, and coinage metals turns out to be a significant challenge to present day semilocal density functionals. The deficiencies of semilocal functionals can be summarized as follows. (i) Using the PBE functional, the 3d lattice constants are slightly too small, and the 4d and 5d lattice constants are too large. (ii) Furthermore, the difference to the experimental volumes shows an upwards slope with increasing d-band filling for 4d and 5d metals. Since other semilocal functionals, for instance PBEsol, reduced the volume by roughly the same magnitude for all metals, none of the semilocal functionals gives a satisfactory description.

The meta-GGA functional revTPSS yields essentially identical results as the PBEsol functional from half filling on, but improves significantly upon the PBEsol functional for less than half filling. By rectifying issue (ii), the revTPSS functional yields the best lattice constants for 4d and 5d metals, with sizable errors only prevailing for the alkali metals. The volume error for the alkali metals using semilocal functionals is related to the neglect of dispersion forces related to the semicore s and p states, an issue that has already been partly resolved in Ref. 16 using pairwise corrections. Unfortunately, issue (i), the underestimation of the lattice constants of 3d metals, remains unaddressed by the revTPSS functional.

As previously observed, the optB88-vdW functional seems to overestimate the dispersion forces in the alkali and alkaline earth metals and gives lattice constants that are too short at the beginning of the series. Furthermore, towards the

TABLE III. Theoretical atomization energies in eV for PBE, PBEsol, revTPSS, and RPA. The atomic electron configuration considered as starting point for the RPA calculations is reported in the second column. The lowest atomic electronic configuration of Ti for the DFT functionals is $3d^34s^1$. The electronic configurations of V and W also differ from experiment (experiment: V $3d^34s^2$, W $5d^46s^2$). The "Error" columns report the absolute error with respect to experiment. The last column reports the experimental values corrected for phonon zero-point vibrational effects (uncorrected values are in parentheses). The estimated error bar for the atomization energies of the DFT and RPA calculations (technical convergence with respect to all parameters) is ± 20 meV and ± 50 meV, respectively.

	Configuration	PBE	Error	PBEsol	Error	revTPSS	Error	RPA	Error	Experiment
K	$4s$	0.87	−0.07	0.93	−0.01	0.97	0.03	0.86	−0.08	0.94[a] (0.93)[a]
Ca	$4s^2$	1.91	0.05	2.12	0.26	2.06	0.20	1.51	−0.35	1.86 (1.84)[b]
Sc	$3d4s^2$	4.11	0.18	4.54	0.61	4.30	0.37	3.75	−0.18	3.93 (3.90)[b]
Ti	$3d^24s^2$	5.27	0.39	5.83	0.95	5.58	0.70	4.98	0.10	4.88 (4.85)[b]
V	$3d^44s^1$	5.37	0.03	5.97	0.63	5.80	0.46	5.24	−0.10	5.34 (5.31)[b]
Fe	$3d^64s^2$	4.89	0.59	5.66	1.36	5.24	0.94	4.20	−0.10	4.30 (4.28)[b]
Co	$3d^74s^2$	4.98	0.56	5.79	1.37	5.38	0.96	4.52	0.10	4.42 (4.39)[b]
Ni	$3d^84s^2$	4.75	0.27	5.46	0.98	5.24	0.76	4.00	−0.48	4.48 (4.44)[b]
Cu	$3d^{10}4s^1$	3.50	−0.02	4.06	0.54	4.16	0.64	3.33	−0.19	3.52[c] (3.49)[c]
Rb	$5s$	0.77	−0.09	0.84	−0.02	0.86	0.00	0.83	−0.03	0.86 (0.85)[b]
Sr	$5s^2$	1.61	−0.12	1.81	0.08	1.81	0.08	1.50	−0.23	1.73 (1.72)[b]
Y	$4d5s^2$	4.16	−0.23	4.60	0.21	4.46	0.07	4.04	−0.35	4.39 (4.37)[b]
Zr	$4d^25s^2$	6.19	−0.08	6.84	0.57	6.53	0.26	6.14	−0.13	6.27 (6.25)[b]
Nb	$4d^45s^1$	6.96	−0.63	7.67	0.08	7.51	−0.08	6.97	−0.62	7.59 (7.57)[b]
Mo	$4d^55s^1$	6.28	−0.56	7.09	0.25	6.91	0.07	6.60	−0.24	6.84 (6.82)[b]
Tc	$4d^55s^2$	6.88	0.00	7.82	0.94	7.46	0.58	6.94	0.06	6.88 (6.85)[b]
Ru	$4d^75s^1$	6.70	−0.07	7.75	0.98	7.20	0.43	6.61	−0.16	6.77 (6.74)[b]
Rh	$4d^85s^1$	5.70	−0.08	6.65	0.87	6.28	0.50	5.44	−0.34	5.78[c] (5.75)[c]
Pd	$4d^{10}$	3.76	−0.18	4.50	0.56	4.46	0.52	3.44	−0.50	3.94[c] (3.91)[c]
Ag	$4d^{10}5s^1$	2.52	−0.46	3.09	0.11	3.05	0.07	2.63	−0.35	2.98[c] (2.96)[c]
Cs	$6s$	0.72	−0.09	0.78	−0.03	0.83	0.02	0.81	0.00	0.81 (0.80)[b]
Ba	$6s^2$	1.88	−0.03	2.12	0.21	2.09	0.18	1.75	−0.16	1.91 (1.90)[b]
Hf	$5d^26s^2$	6.42	−0.04	7.08	0.62	6.95	0.49	6.20	−0.26	6.46 (6.44)[b]
Ta	$5d^36s^2$	8.11	−0.01	8.93	0.81	8.83	0.71	7.88	−0.24	8.12 (8.10)[b]
W	$5d^56s^1$	8.39	−0.53	9.17	0.25	9.17	0.25	8.53	−0.39	8.92 (8.90)[b]
Re	$5d^56s^2$	7.80	−0.25	8.77	0.72	8.69	0.64	7.76	−0.29	8.05 (8.03)[b]
Os	$5d^66s^2$	8.34	0.14	9.42	1.22	9.19	0.99	8.19	−0.01	8.20 (8.17)[b]
Ir	$5d^76s^2$	7.31	0.34	8.35	1.38	8.09	1.12	7.03	0.06	6.97 (6.94)[b]
Pt	$5d^96s^1$	5.51	−0.35	6.38	0.52	6.27	0.41	5.06	−0.80	5.86 (5.84)[b]
Au	$5d^{10}6s^1$	3.05	−0.78	3.74	−0.09	3.67	−0.16	3.12	−0.71	3.83 (3.81)
ME			−0.07		0.56		0.41		−0.23	
MAE			0.24		0.57		0.42		0.25	

[a]Reference 4.

[b]Reference 34.

[c]Reference 32.

right of the periodic table, the functional essentially recovers the PBE results. Hence, the trend (ii) to overestimate the equilibrium volumes with increasing d-band filling is even more pronounced for optB88-vdW than for either PBE or PBEsol, a point that needs to be addressed in the future in order to make vdW functionals fully competitive.

The RPA results for lattice constants of 4d and 5d metals are remarkably close to the revTPSS results, but since the RPA includes dispersion forces, outliers (errors for the alkali metals) are not present, supporting our claim that the RPA accounts equally well for all bonding situations. Furthermore, the RPA results for the 3d metals are in good agreement with experiment and do not show the peculiar underestimation of the volume observed for standard density functionals.

For the atomization energies, we find that the RPA and PBE perform roughly equally, although the RPA trend towards too weak binding, as for other solids and molecules, prevails. PBEsol and revTPSS atomization energies are very similar and significantly too large compared to experiment. Overall, RPA offers a well-balanced description with mean absolute errors being smaller than for the density functionals considered here.

*laurids.schimka@univie.ac.at

[1] P. Hohenberg and W. Kohn, Phys. Rev. B **136**, 864 (1964).

[2] W. Kohn and L. J. Sham, Phys. Rev. **140**, A1133 (1965).

[3] P. Haas, F. Tran, and P. Blaha, Phys. Rev. B **79**, 085104 (2009).

[4] G. I. Csonka, J. P. Perdew, A. Ruzsinszky, P. H. T. Philipsen, S. Lebègue, J. Paier, O. A. Vydrov, and J. G. Ángyán, Phys. Rev. B **79**, 155107 (2009).

[5] J. P. Perdew, K. Burke, and M. Ernzerhof, Phys. Rev. Lett. **77**, 3865 (1996).

[6] J. P. Perdew, A. Ruzsinszky, G. I. Csonka, O. A. Vydrov, G. E. Scuseria, L. A. Constantin, X. Zhou, and K. Burke, Phys. Rev. Lett. **100**, 136406 (2008).

[7] J. P. Perdew, A. Ruzsinszky, G. I. Csonka, L. A. Constantin, and J. Sun, Phys. Rev. Lett. **103**, 026403 (2009).

[8] J. Sun, M. Marsman, G. I. Csonka, A. Ruzsinszky, P. Hao, Y.-S. Kim, G. Kresse, and J. P. Perdew, Phys. Rev. B **84**, 035117 (2011).

[9] J. Klimeš, D. R. Bowler, and A. Michaelides, J. Phys.: Condens. Matter **22**, 022201 (2010).

[10] M. Dion, H. Rydberg, E. Schröder, D. C. Langreth, and B. I. Lundqvist, Phys. Rev. Lett. **92**, 246401 (2004).

[11] D. C. Langreth and J. P. Perdew, Solid State Commun. **17**, 1425 (1975).

[12] O. Gunnarsson and B. I. Lundqvist, Phys. Rev. B **13**, 4274 (1976).

[13] D. C. Langreth and J. P. Perdew, Phys. Rev. B **15**, 2884 (1977).

[14] G. Kresse, J. Furthmüller, and J. Hafner, Europhys. Lett. **32**, 729 (1995).

[15] J. Hafner, *From Hamiltonians to Phase Diagrams* (Springer, Berlin, 1987), p. 34.

[16] J. Tao, J. P. Perdew, and A. Ruzsinszky, Phys. Rev. B **81**, 233102 (2010).

[17] T. Qin, R. Drautz, and D. G. Pettifor, Phys. Rev. B **78**, 214108 (2008).

[18] J. Sánchez-Barriga, J. Fink, V. Boni, I. Di Marco, J. Braun, J. Minár, A. Varykhalov, O. Rader, V. Bellini, F. Manghi, H. Ebert, M. I. Katsnelson, A. I. Lichtenstein, O. Eriksson, W. Eberhardt, and H. A. Dürr, Phys. Rev. Lett. **103**, 267203 (2009).

[19] S. Monastra, F. Manghi, C. A. Rozzi, C. Arcangeli, E. Wetli, H.-J. Neff, T. Greber, and J. Osterwalder, Phys. Rev. Lett. **88**, 236402 (2002).

[20] J. Braun, J. Minár, H. Ebert, M. I. Katsnelson, and A. I. Lichtenstein, Phys. Rev. Lett. **97**, 227601 (2006).

[21] A. V. Narlikar, *Frontiers in Magnetic Materials* (Springer, Berlin, 2005), p. 117.

[22] J. Harl and G. Kresse, Phys. Rev. B **77**, 045136 (2008).

[23] J. Harl and G. Kresse, Phys. Rev. Lett. **103**, 056401 (2009).

[24] J. Harl, L. Schimka, and G. Kresse, Phys. Rev. B **81**, 115126 (2010).

[25] A. Gruneis, M. Marsman, J. Harl, L. Schimka, and G. Kresse, J. Chem. Phys. **131**, 154115 (2009).

[26] G. Kresse and J. Hafner, Phys. Rev. B **48**, 13115 (1993).

[27] G. Kresse and J. Furthmüller, Comput. Mater. Sci. **6**, 15 (1996).

[28] P. E. Blöchl, Phys. Rev. B **50**, 17953 (1994).

[29] G. Kresse and D. Joubert, Phys. Rev. B **59**, 1758 (1999).

[30] J. Paier, M. Marsman, K. Hummer, G. Kresse, I. C. Gerber, and J. G. Ángyán, J. Chem. Phys. **124**, 154709 (2006).

[31] G. Kresse and J. Hafner, J. Phys.: Condens. Matter **6**, 8245 (1994).

[32] L. Schimka, J. Harl, and G. Kresse, J. Chem. Phys. **134**, 024116 (2011).

[33] G. Steinle-Neumann, L. Stixrude, and R. E. Cohen, Phys. Rev. B **60**, 791 (1999).

[34] Ch. Kittel, *Einführung in die Festkörperphysik* (Oldenbourg, München, 1983), p. 92.

[35] *Interaction of Charged Particles and Atoms with Surfaces*, Landolt-Börnstein-Group III Condensed Matter, edited by G. Chiarotti, Vol. 24c (Springer, Berlin, Heidelberg, 1995).

[36] D. Hobbs, J. Hafner, and D. Spišák, Phys. Rev. B **68**, 014407 (2003).

[37] A. D. Becke, Phys. Rev. A **38**, 3098 (1988).

[38] J. Klimeš, D. R. Bowler, and A. Michaelides, Phys. Rev. B **83**, 195131 (2011).

[39] S. H. Vosko, L. Wilk, and M. Nusair, Can. J. Phys. **58**, 1200 (1980).